International Journal of Steel Structures (2022) 22(4):1175–1188
https://doi.org/10.1007/s13296-022-00628-9

Online ISSN 2093-6311
Print ISSN 1598-2351

Behaviour of CFST Stub Columns Subjected to Pure Compression

A. Horváth[1] · **D. Kollár**[1] · **B. Kövesdi**[1]

Received: 17 April 2022 / Accepted: 14 June 2022 / Published online: 2 July 2022

Abstract
Application of concrete-filled steel tubes (CFST) is becoming increasingly prominent in the civil engineering practice. However, the interaction of cross-sectional elements in CFST columns raises a number of questions, which have to be investigated in detail to improve design background and analytical resistance formulae. The aim of the current paper is to examine the structural behaviour of innovative concrete-filled steel tubes using different structural steel grades (S355, S500 and S960) and concrete classes (C30/37 and C60/75). Combination of normal or high strength steel with normal or high-performance concrete is a novel research topic of composite structures resulting in economic and optimal design for distinct civil engineering applications such as buildings, bridges, towers and masts, etc. An advanced finite element model is developed and validated based on previous experimental results found in the international literature in order to investigate the discrepancies in structural behaviour, load-bearing capacity and failure mode of stub columns subjected to pure compression. Validated numerical results are compared to formulae-based resistances and the applicability of standardised design methods are examined. In addition, a novel formula is proposed considering hardening of steel material in accordance with EN 1993-1-5. The developed formula can be used for the economic design of CFST stub columns, combining normal and high strength materials, where elastic shell buckling cannot occur ($D/t \leq 90\varepsilon^2$).

Keywords Concrete-filled steel tube · Normal strength steel · High strength steel · Composite · Finite element analysis

1 Introduction

Over the past two decades, application of concrete-filled steel tubes (CFST) has increased considerably in the civil engineering practice, while CFST sections have undergone a major development since they are a competitive alternative to conventional steel or reinforced concrete columns. The primary reason for the appearance of concrete-filled steel tubes was to reduce cross-sectional dimensions of columns, in parallel with increasing the load-bearing capacity (Han et al., 2014). Concrete-filled steel tubes have gained a dominant role in buildings and bridges internationally, especially in China, and as a result, there has been an exponential growth in the last decade in terms of the range of applications and different structural designs. In high-rise buildings, CFST elements are usually used as columns connected to some non-composite (steel or reinforced concrete) elements. The appearance of concrete-filled steel sections in bridge constructions can be observed in several structural systems. CFST elements can be found in piles of cable-stayed and suspension bridges or in truss bridges, but their presence in bridge construction is most significant in arch bridges. More than 400 bridges have been built using this innovative structural system in the last twenty years in China. Five of the ten arch bridges with the largest spans have concrete-filled steel tube sections (CFST, 2022). In addition, the Third Pingnan Bridge, built with CFST elements, is at the top of the list with a total length of 1035 m and a main span of 575 m. La Vicaria tied arch bridge in Spain was opened to traffic in 2007 with a total length of 260 m and a span of 168 m. The bridge arch is built with a polygonal CFST cross-section and is one of the few European applications of concrete-filled steel sections. Concrete-filled steel tubes columns can also be used for metro station columns, utility poles, transmission towers and wind turbines (Han et al., 2014). Examples of different applications are shown in Fig. 1.

Steel tubes filled with concrete are characterised by using a variety of materials (normal strength materials (Abramski,

✉ D. Kollár
kollar.denes@emk.bme.hu

[1] Faculty of Civil Engineering, Department of Structural Engineering, Budapest University of Technology and Economics, Műegyetem rkp. 3, Budapest 1111, Hungary

Fig. 1 Application of CFST elements in **a** high-rise buildings (Canton Tower, 2022) and **b** footbridges and **c** road bridges (La Vicaria bridge 2022)

2018; Zhang et al., 2019), high-strength materials (Yan et al., 2019, 2021a), fibre-reinforced concrete (Tretyakov et al., 2021), self-compacting concrete (Huang et al., 2022; Li et al., 2020), stainless steel (He et al., 2021; Ye et al., 2021), etc.) and cross-sectional shapes (circular (Avci-Karatas, 2019, 2021; Han et al., 2014), elliptical (Ren et al., 2014), polygonal (Hassanein et al., 2017, etc.), allowing the design of architecturally aesthetic, slender structures. The most common and oldest design is the circular cross-section. Concrete-filled steel tubes have a wide range of practical applications resulting in the use of new cross-section types. Many research studies consider the behaviour of circular CFSTs as a reference when investigating other types of cross-sectional shapes (Ayough et al., 2021; Zhao et al., 2018). Square and rectangular cross-sections are becoming increasingly common in the construction industry (Dong et al., 2018), due to the simpler design of column-beam connections, the significant bending resistance of the cross-section and aesthetic considerations. However, rectangular cross-sections have the disadvantage that local buckling resistance is lower than circular ones and the confinement effect of the steel section, resulting in increased concrete strength, is less significant (Zhao et al., 2018). The use of high strength steels (above yield strength of 360 MPa according to ISO TR 15608) and ultra-high strength steels (above yield strength of 690 MPa) makes it possible to reduce wall thickness of steel sections and to minimise material consumption. On the other hand, increased yield strength increases the risk of local buckling (Yan et al., 2021a). In addition, load bearing capacity and behaviour at both low and elevated temperature have been investigated in the past years (Romero et al., 2020; Yan et al., 2019, 2021b; Yu et al., 2019). In the majority of papers, compressive behaviour has been investigated; however, structural behaviour under tension, torsion and bending has been already analysed in some cases (Elchalakani et al., 2001; Han et al., 2007, 2016; Le et al., 2021; Ye et al., 2021).

A comprehensive literature review is conducted to summarize the directives of design standards and design proposals based on experiments and numerical studies regarding the load-bearing capacity of CFST stub columns subjected to pure compression. Determination of the load-bearing capacity is a complex task due to interaction of cross-sectional elements. Consideration or negligence of this effect results in significant differences in resistance, while dealing with this phenomenon in design procedures and numerical simulations is an important issue. Therefore, advanced nonlinear

three-dimensional finite element models are developed and validated for simulating the fundamental phenomena of concrete-filled steel tubes with circular hollow sections.

2 Literature Review

Experimental studies are essential to understand the structural behaviour of concrete-filled steel tubes. Laboratory test can be aimed at extending available experimental results, evaluating and developing design formulae or providing sufficient data to develop numerical models. In addition to laboratory tests, numerical modelling can also be a useful tool to extend experimental results, modelling geometric properties and other conditions that would be lengthy, difficult or even impossible to investigate experimentally (Abed et al., 2013). Design standards, as well as various recommendations and formula development in the international literature, can help in everyday design tasks. Concrete-filled steel tubes are mostly used as compressed elements in civil engineering practice. In the following, the current paper summarises both experimental and numerical results of previous studies of CFST stub columns subjected to pure compression, while design proposals for analytical calculations are introduced as well. Typical notations for CFST stub columns are shown in Fig. 2, where t is wall thickness, D is outer diameter, D_i is inner diameter, while L is column length.

Ellobody et al. (2006) conducted laboratory tests to investigate the behaviour of axially loaded normal and high strength concrete-filled compact steel tube circular stub

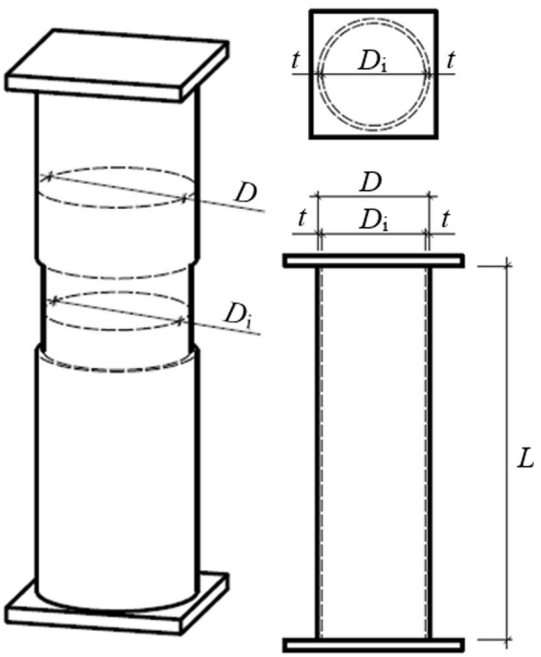

Fig. 2 Notations for CFST stub columns used in the paper

columns with a wide range of concrete cube strengths varying between 30 to 110 MPa and D/t ranging from 15 to 80. They concluded that design approaches in American Specifications and Australian Standards are conservative, while Eurocode 4 is in general unconservative. On the other hand, American Specifications and Australian Standards are capable of predicting reliable results when the contribution of concrete to the axial resistance is multiplied by a reduction factor of 0.85. An experimental program was carried out by Abed et al. (2013) at the American University of Sardinia in 2013 involving laboratory testing of CFST specimens and steel tubes. The CFST specimens were designed using normal and high strength concrete, using normal strength steel tubes. In all cases, the diameter-to-length ratio of the specimens was $D/L = 2$, and the tube diameter-to-wall thickness ratio was $D/t = 20$, 32 and 54. Tests were carried out on a universal test machine with a load capacity of 3000 kN, while strain gauges were installed on specimens in order to monitor axial and circumferential strains during testing. They concluded that higher concrete strength results in significantly higher axial compressive strength, and an increase in D/t ratio decreases the axial strength of CFST elements, which is primarily governed by the reduction of compressive concrete strength due to less confinement. Experimental investigations were also performed by Ibañez et al. (2021) in 2021. Eighteen CFST stub columns, using high strength concrete, were tested under axial compression to extend the available experimental data. Different wall thickness and cross-sectional shapes were examined. Concrete classes used in the tests were C30 and C90 combined with hollow sections made of S275 and S355 structural steel grade. They concluded that specimens filled with high strength concrete and those with smaller wall thickness showed less ductility. In 2021, Yan et al. (2021a) tested twenty-three ultra-high performance concrete-filled Q690 high-strength steel tubes at low temperatures, between − 80 and + 30 °C, concluding that decreasing temperature resulted in improved ultimate compressive resistance.

In 2003, Hu et al. (2003) carried out numerical analyses of CFST specimens. They used 27-node solid elements for both sectional parts in the finite element model. Due to symmetry, only one eighth of the CFST column was analysed with the appropriate boundary conditions. They concluded that circular steel tubes can provide good confining effect especially when the diameter-to-wall thickness ratio is small ($D/t < 40$). Furthermore, square sections are not effective in providing large confining effect when the width-to-thickness ratio is large ($D/t > 40$). Abed et al. (2013) performed numerical studies in addition to their experimental research. The modelled specimen was a circular concrete-filled steel tube with end plates. The concrete and steel parts were modelled using eight-node solid elements, except the end plates which were modelled using rigid elements. Surface-to-surface

contact are used to model the interaction between concrete and steel elements of the specimen, with tangential and normal contact definitions. For the definition of the concrete infill material, an equivalent stress–strain curve, which theory was invented by Ellobody et al. (2006), and concrete damaged plasticity model were used. The investigation showed that there is an insignificant deviation between using solid and shell elements. In 2019, Patel et al. (2019) presented axisymmetric simulations, using four-node axisymmetric quadrilateral elements with reduced integration, to model circular CFST with ultra-high performance concrete (UHPC) and performed a parametric study investigating the effect of D/t ratio. They concluded that the proposed axisymmetric model is much simpler than detailed three-dimensional model, and also predicts the behaviour of axially loaded circular CFST stub columns with fair precision. The parametric study revealed that the steel contribution ratio greater than 0.3 and $D/t < 30$ should be maintained to ensure sufficient ductility of CFST columns with UHSC. In addition, they concluded that the application of UHPC in CFST columns approximately reduces the cross-sectional size by 50% when compared with the use of normal strength concrete. Ayough et al. (2021) performed numerical analyses in 2021 using circular, square, hexagonal and octagonal cross-sectional shapes. An idealized five-stage stress–strain curve was applied for steel, while Drucker-Prager plasticity model and confined concrete stress–strain curve were used for concrete. Different cross-sections have varying confinement effect. Based on the numerical simulations they concluded the effect of residual stresses on the behaviour of CFST stub columns is negligible, while octagonal and hexagonal CFST columns show better ductility than the square ones. On the other hand, confinement effect provided by square sections was found to be significantly smaller than that by the circular steel tubes.

Several design standards and design proposals in the literature are available for the analytical calculation of compressive load-bearing capacity of CFST elements. Theoretical load-bearing capacity N_{theory} based on the theory of composite structures according to Abed et al. (2013), ignoring the increase of concrete compressive strength due to triaxial loading, yields the equation given by Eq. 1.

$$\mathrm{N}_{theory} = \mathrm{A_a f_y} + \mathrm{A_c f_c} \tag{1}$$

where A_a and A_c are cross-sectional areas, f_y and f_c are yield strength and compressive strength for steel and concrete parts, respectively. Specifications of the American Concrete Institute (ACI 318-11) and Australian Standard (AS 3600) recommend using Eq. 2 for design.

$$\mathrm{N}_{ACI/AS} = \mathrm{A_a f_y} + 0.85\mathrm{A_c f_c} \tag{2}$$

Giakoumelis and Lam (2004) proposed a coefficient (Eq. 3) for the analytical equation recommended in ACI/AS standards to take the effect of concrete confinement into account on the ultimate axial load-bearing capacity N_u of concrete-filled steel tubes based on experiments.

$$\mathrm{N}_u = \mathrm{A_a f_y} + 1.3\mathrm{A_c f_{ck}} \tag{3}$$

Mander et al. (1989) developed a formula (Eq. 4) by defining compressive strength of confined concrete f_{cc} (Eqs. 5–7).

$$\mathrm{N}_{Mander} = \mathrm{A_a f_y} + \mathrm{A_c f_{cc}} \tag{4}$$

$$f_{\mathrm{cc}} = \mathrm{f_c}\left(-1.254 + 2.254\sqrt{1+\frac{7.94\mathrm{f_l}}{\mathrm{f_c}}} - 2\frac{\mathrm{f}_l}{\mathrm{f_c}}\right) \tag{5}$$

where

$$\mathrm{f_l} = \frac{2\sigma_\theta \mathrm{t}}{\mathrm{D}} \tag{6}$$

and

$$\sigma_\theta = 0.1\mathrm{f_y} \tag{7}$$

The EN 1994-1-1 standard (EN 1994-1-1) gives guidance on the verification of CFST elements taking the increase in compressive strength of concrete caused by confinement. Plastic resistance to compression N_{EC} according to Eurocode can be calculated using Eq. 8, where $\eta_a = 0.25\left(3 + 2\bar{\lambda}\right)$ and $\eta_c = 4.9 - 18.5\bar{\lambda} + 17\bar{\lambda}^2$ for centrally loaded elements, while $\bar{\lambda}$ is relative slenderness and material properties are considered by their design values (f_{yd} and f_{cd}).

$$\mathrm{N}_{EC} = \eta_a \mathrm{A_a f_{yd}} + \left(1 + \eta_c \frac{\mathrm{t}}{\mathrm{D}}\frac{\mathrm{f_y}}{\mathrm{f_{ck}}}\right)\mathrm{A_c f_{cd}} \tag{8}$$

A comprehensive literature review is carried out focusing on previous experimental and numerical results of CFST stub columns subjected to pure compression, while different design approaches and proposals are summarized as well. However, it can be concluded that there are only a small number of studies available which summarise and compare the effect of widely varying material properties, especially combining normal and high strength materials, and different diameter-to-wall thickness parameters to design formulae found in the literature, which shows the novelty and relevance of the current study.

3 Development of Numerical Model

Advanced three-dimensional finite element model is developed in ABAQUS, a general-purpose finite element software, in order to take geometrical and material nonlinearities into account during axial loading of normal and high

strength material CFST stub columns with circular cross-section. The major importance of the developed numerical model is investigating the influence of using normal and high strength steel (S355, S500 and S960) and normal and high-performance concrete (C30/37 and C60/75) to examine the structural behaviour of innovative concrete-filled steel tubes with multiple wall thickness and diameter-to-wall thickness ratio. Table 1 summarizes the main dimensions and material properties of analysed specimens presented in the current paper. Three specimens, with diameters $D = 114$ mm and 167 mm, wall thicknesses $t = 3.1$ mm, 3.6 mm and 5.6 mm, length $L = 250$ mm, yield strength $f_y = 310$ MPa and compressive strength $f_{ck} = 60$ MPa, in the list are references for model validation and was tested by Abed et al. (2013). The first number in specimen notations indicate yield strength of the steel tube and the second number denotes the concrete compressive strength. A total of twelve specimens are considered in the parametric analysis assuming wall thickness of both 3 mm and 5.6 mm.

The concrete core and the steel tube are modelled using linear eight-node solid elements (finite element type C3D8R in the software) with reduced integration since smaller low-order elements perform better than larger high-order elements in nonlinear problems (Michaleris, 2011). The solid element has three degrees of freedom per node. An essential step in modelling is to specify the contact elements between concrete and steel tube. The interaction definition is based on the numerical studies by Abed et al. (2013) and Tao et al. (2013). Accordingly, surface-to-surface contact is adopted in the numerical simulation using tangential and normal contact. Penalty-based method is applied for the tangential frictional behaviour, with friction coefficient of 0.3 as recommended in the literature, with finite sliding. On the other hand, hard contact is used to describe the normal contact behaviour allowing separation. Typical finite element mesh of a CFST is shown in Fig. 3. The total number of nodes and elements are 10,404 and 6800 for the steel tube and 2938 and 2400 for the concrete infill, respectively. A mesh sensitivity analysis is carried out in order to determine the adequate finite element mesh for evaluating the load-bearing capacity and failure mode. Therefore, two solid elements are defined along the wall thickness of the steel tube, while a mesh size of 5 mm is used in the axial direction for both concrete and steel parts and finite element size of ~ 10 mm is used in cross-sectional terms.

End plates of the CFST is modelled with analytical rigid parts and master nodes. It allows the required constraints and loads to be defined directly at each master node at the ends. Supports prevent transverse displacements (U_X and U_Y) and rotation of the cross-section in all directions. In the axial direction, an elastic lower support with a spring constant of 1000 kN/mm is defined in the model based on the experimental setup of pure steel tubes in Abed et al. (2013) in order to take the stiffness of testing device into account and evaluate initial structural stiffness accurately. On the other hand, prescribed axial displacement ($U_Z = 60$ mm) acting at the centre of the upper cross-section is used for loading.

Definition of proper material models is essential in modelling and one of the key parameters of the load-carrying capacity. Multilinear isotropic hardening material models with von Mises yield criterion and associative flow rule are defined for normal strength ($f_y = 310$ MPa and 355 MPa) and high strength steel (0.2% proof strength $f_{p0.2} = 500$ MPa and 960 MPa) as well. Tensile test results introduced in Abed et al. (2013) are used for validation in the case of $f_y = 310$ MPa. Young's modulus E is 200 GPa and Poisson's ratio ν is 0.3 in all the cases. In the parametric analysis, different material models are used for normal strength and high strength steels. A quad-linear material model, as given by Eqs. 9–14, which has been proposed in prEN 1993-1-14 (2020) is applied to capture yield plateau and strain-hardening behaviour of normal strength steels.

$$\sigma(\varepsilon) = \begin{cases} \mathrm{E}\varepsilon, & \varepsilon \le \varepsilon_y \\ \mathrm{f_y}, & \varepsilon_y < \varepsilon \le \varepsilon_{sh} \\ \mathrm{f_y} + \mathrm{E_{sh}}\left(\varepsilon - \varepsilon_{sh}\right), & \varepsilon_{sh} < \varepsilon \le \mathrm{C_1}\varepsilon_u \\ \mathrm{f_y C_1}\varepsilon_u + \frac{\mathrm{f_u} - \mathrm{f_y C_1}\varepsilon_u}{\left(\varepsilon_u - \mathrm{C_1}\varepsilon_u\right)}\left(\varepsilon - \mathrm{C_1}\varepsilon_u\right), & \mathrm{C_1}\varepsilon_u < \varepsilon \le \varepsilon_u \end{cases} \quad (9)$$

Table 1 Dimensions and material properties of analysed specimens

Purpose of analysis	Specimen#	D (mm)	t (mm)	L (mm)	D/t	f_y (MPa)	f_{ck} (MPa)
Validation	310-60-3.1	167	3.1	250	54	310	60
	310-60-3.6	114	3.6	250	32	310	60
	310-60-5.6	114	5.6	250	20	310	60
Parametric study	355-30-3/5.6	114	3/5.6	250	20/38	355	30
	500-30-3/5.6	114	3/5.6	250	20/38	500	30
	960-30-3/5.6	114	3/5.6	250	20/38	960	30
	355-60-3/5.6	114	3/5.6	250	20/38	355	60
	500-60-3/5.6	114	3/5.6	250	20/38	500	60
	960-60-3/5.6	114	3/5.6	250	20/38	960	60

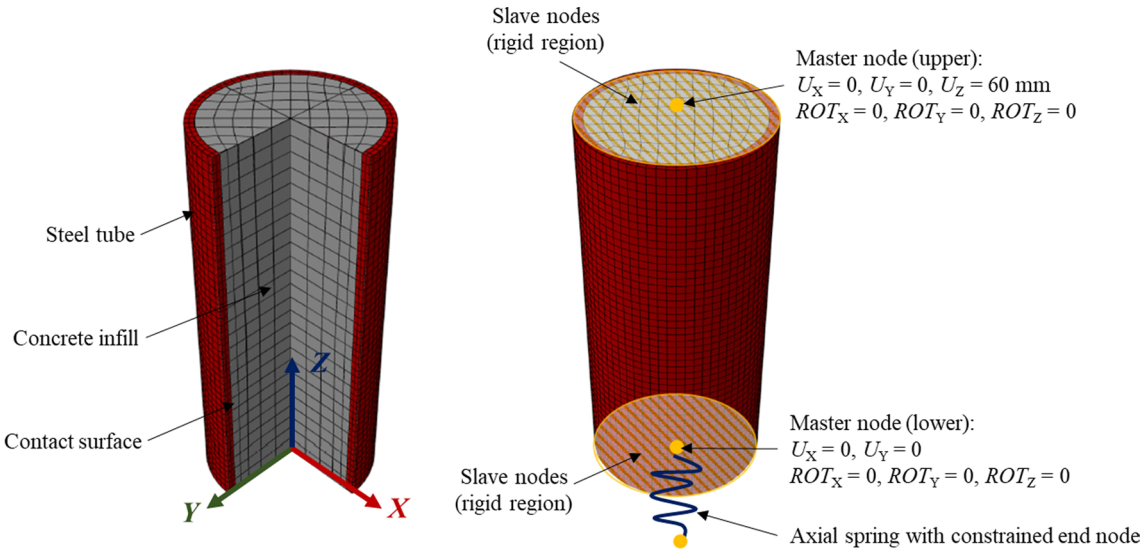

Fig. 3 Finite element mesh and boundary conditions of the CFST stub column

$$E_{sh} = \frac{f_u - f_y}{C_2\varepsilon_u - \varepsilon_{sh}} \tag{10}$$

$$\varepsilon_{sh} = 0.1\frac{f_y}{f_u} - 0.055 \quad 0.01 \le \varepsilon_{sh} \le 0.03 \tag{11}$$

$$\varepsilon_u = 0.6\left(1 - \frac{f_y}{f_u}\right) 0.06 \le \varepsilon_u < A = 0.20 \tag{12}$$

$$C_1 = \frac{\varepsilon_{sh} + 0.25(\varepsilon_u - \varepsilon_{sh})}{\varepsilon_u} \tag{13}$$

$$C_2 = \frac{\varepsilon_{sh} + 0.4(\varepsilon_u - \varepsilon_{sh})}{\varepsilon_u} \tag{14}$$

Ramberg–Osgood material model is used to model high strength steels. Relation between strain ε and stress σ is described with $\varepsilon = \frac{\sigma}{E} + 0.002\left(\frac{\sigma}{f_{p0.2}}\right)^n$, where n can be taken as 14 for high strength steels based on the material tests of Somodi (Somodi, 2018). Applied stress–strain curves of normal and high strength steels are shown in Fig. 4.

Similarly to steel, multilinear isotropic hardening material models are defined for normal strength ($f_{ck} = 30$ MPa) and high strength concrete ($f_{ck} = 60$ MPa). The compressive strength f_{ck} of unconfined concrete is the uniaxial compressive strength on cylinder. Behaviour of confined concrete differs significantly (Fig. 5) since concrete compressive strength increases due to triaxial loading as steel tube prevents lateral expansion of the concrete core. Therefore, a modified isotropic model is used to consider confinement

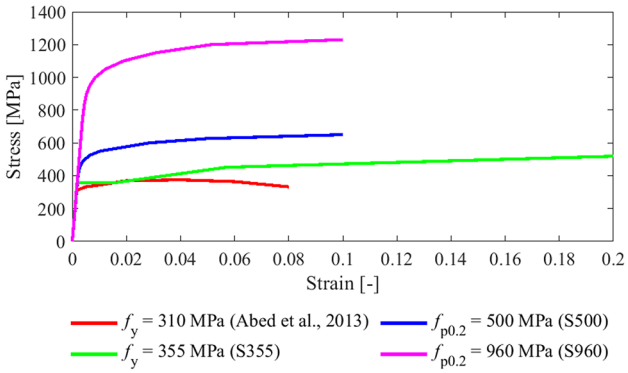

Fig. 4 Stress–strain curves of applied structural steels

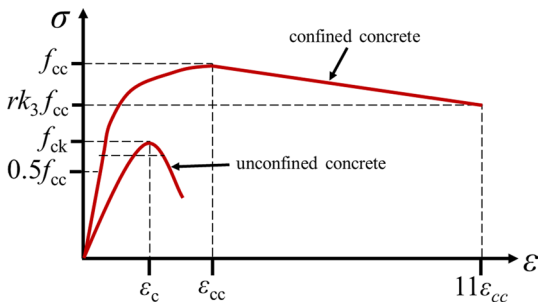

Fig. 5 Parametric stress–strain curves of confined and unconfined concrete based on Ellobody et al. (2006)

effect. Definition of stress–strain curves for confined concrete are based on Ellobody et al. (2006). Confined concrete shows linear behaviour up to $0.5f_{cc}$, where f_{cc} is confined concrete strength. Hu et al. (2003) proposed to calculate

confined concrete strength using $f_{cc} = f_{ck} + k_1 f_1$, where f_{ck} is uniaxial cylinder compressive strength (corresponding strain is $\varepsilon_c = 0.003$), f_1 is effective lateral confining stress on the concrete core calculated using Eq. 6, while corresponding increased strain of confined concrete is $\varepsilon_{cc} = \varepsilon_c\left(1 + k_2 \frac{f_1}{f_{ck}}\right)$. Material parameters k_1 and k_2 are 4.1 and 20.5, respectively in the analyses. The increased Young's modulus of confined concrete E_{cc} associated with linear behaviour can be calculated using $E_{cc} = 4700\sqrt{f_{cc}}$ MPa. Poisson's ratio is assumed to be 0.2. Definition of nonlinear behaviour after the linear elastic part can be found in Saenz (1964). However, stress–strain points corresponding to stresses $0.5f_{cc}$ and f_{cc} are connected by a linear section in the current paper. The ultimate elongation can be approximated by $11\varepsilon_{cc}$. The stress associated with this point can be calculated using rk_3f_{cc}, where k_3 is 1 according to Ellobody et al. (2006). Parameter r can be assumed to be 1 for concrete cube strength of 30 MPa and 0.5 for concrete cube strength of 100 MPa based on the study by Mursi and Uy (2003). Linear interpolation is used for intermediate concrete strength. The calculated r value is 0.95 for the modelled normal strength concrete material (cube strength is 37 MPa), and it is 0.68 for high strength concrete (cube strength is 75 MPa).

Direct solver is used with implicit time integration scheme in nonlinear static analysis with full Newton–Raphson method. Large deflection effects are included in the analysis, while displacement loads are ramped linearly.

4 Validation of Numerical Model

First, the three-dimensional finite element model developed in ABAQUS is validated based on previous measurements found in the literature. Three CFST specimens, with wall thickness of 3.1 mm, 3.6 mm and 5.6 mm, used for validation purposes are summarized in Table 1. The axial load–displacement curves of finite element models are presented in Fig. 6 in a common diagram with the experimental data provided by Abed et al. (2013). Geometrical and material properties of the centrally loaded CFST stub column are identical to those investigated experimentally by the researchers (using measured properties) and are adopted in the numerical model. The load capacity of the CFST stub columns were interpreted for 5% principal strain of the steel section in accordance with EN 1993-1-5. Based on this criteria, experimental load-bearing capacities are 1880 kN, 1094 kN and 1357 kN, while numerical model-based resistances are 1835 kN, 1088 kN and 1360 kN for the CFST specimens with wall thickness of 3.1 mm, 3.6 mm and 5.6 mm, respectively. Differences are

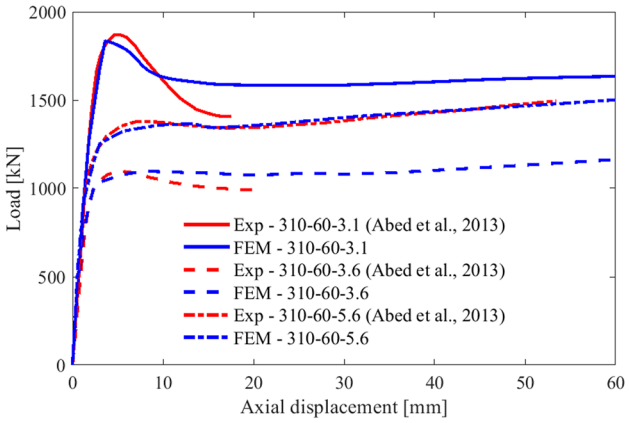

Fig. 6 Experimental ('Exp') (Abed et al., 2013) and finite element model-based ('FEM') axial load–displacement curves for model validation

2.40%, 0.55% and 0.22%, respectively. Load–displacement curves based on the finite element models are in a really good agreement with experimental curves; initial stiffness, load-bearing capacity, displacement corresponding to the load peak and hardening or softening are following measurement data with high accuracy.

In the case of the failure mode (Fig. 7), experiments typically showed the appearance of plastic shell buckling of the steel tube in the lower and upper thirds with axisymmetric buckling shape resulting in axial waves (i.e., dimples), which is also observed in the numerical model (Fig. 7c, d). For some of the experimental specimens, in addition to plastic shell buckling in the lower and upper thirds, plastic buckling was also observed in the mid-height (similarly to Fig. 7b in the finite element model). Additional information is provided by the cross-sections of the finite element models of the failure phenomenon, which clearly shows that the steel tube separates from the concrete core during buckling in the vicinity of lower and upper dimples, while there is contact between concrete and steel in mid-height even after buckling (Fig. 7b).

Axial and hoop strains were measured by Abed et al. (2013) with uniaxial strain gauges during the laboratory tests in the mid-height of the specimens. Displacement readings of the testing machine were synchronized with strain measurement data. Measured and numerical model-based strains are presented in Fig. 8 showing excellent agreement in the designated reference point in the range of published strains. It is shown that axial and hoop strains decrease for specimen '310-60-3.1' when buckling occurs in the mid-height of the specimen (shown in Fig. 7b with contact between steel and concrete ensuring the confinement effect), while hardening can be observed for the other two validated cases where plastic shell buckling only

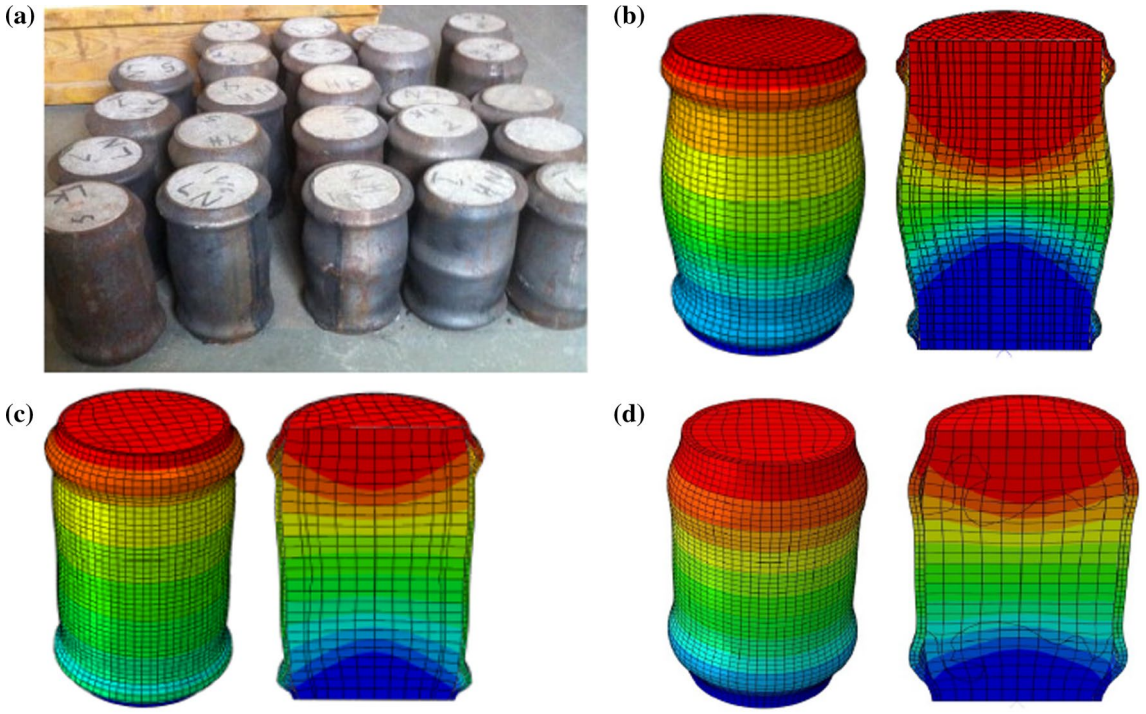

Fig. 7 Failure modes **a** in experiments (Abed et al., 2013) and **b–d** in the finite element models used for validation (310-60-3.1, 310-60-3.6 and 310-60-5.6, respectively)

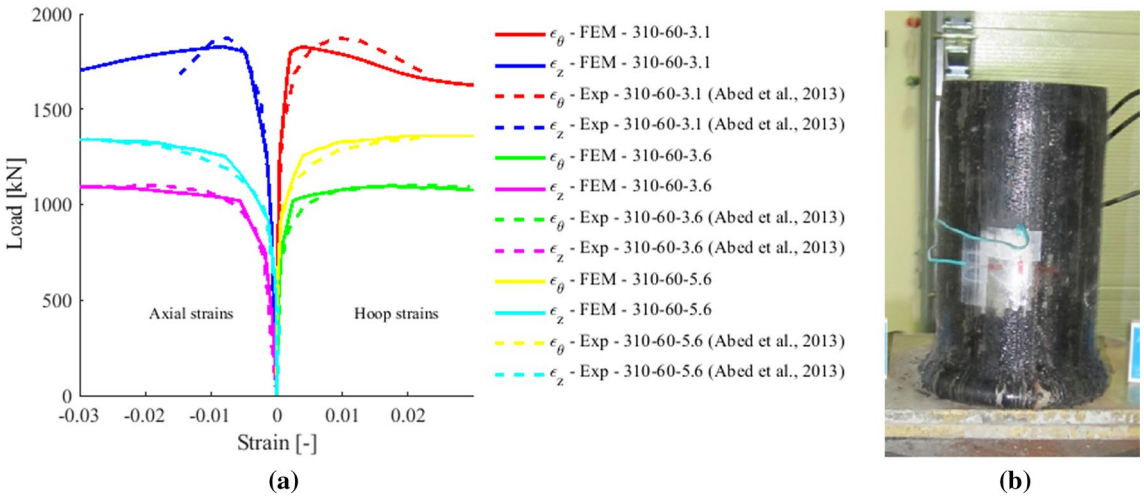

Fig. 8 **a** Axial (ε_z) and hoop (ε_θ) strains in the experiments ('Exp') (Abed et al., 2013) and in the finite element models ('FEM') used for validation and **b** reference point with strain gauges (Abed et al., 2013)

occurs in the vicinity of lower and upper regions (steel and concrete surfaces separate).

After proving the accuracy of the developed numerical model based on test results, it is used for numerical parametric study presented in the following Section to investigate the effect of high strength steel and concrete on the compression resistance.

5 Results of the Numerical Parametric Study

One of the major aims of the paper is to investigate the effect of high strength materials on the load-bearing capacity of centrally loaded CFST stub columns using validated numerical model. The focus of the parametric analysis is on load–displacement curves, load-bearing

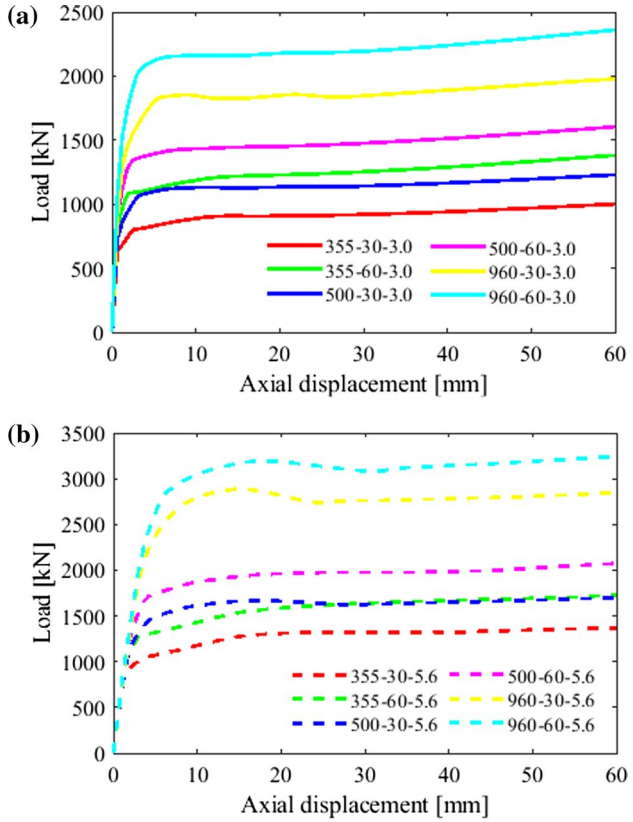

Fig. 9 Axial load–displacement curves in the parametric analysis: **a** t = 3 mm and **b** t = 5.6 mm

capacities and failure modes of each case listed in Table 1. In addition, relationship between design formulae in the literature and standards and the load-bearing capacity predicted by the numerical models are investigated as well. Axial load–displacement curves of the parametric analysis are shown in Fig. 9 studying the effect of the concrete strength, wall thickness and steel yield strength. Steel grades between S235 to S960, concrete strength between 30 and 60 MPa are applied. The wall thickness varies between 3 and 5.6 mm. Based on the results it can be concluded that the increase in concrete strength, yield strength of the steel material of the cross-section and wall thickness increases the load-bearing capacity of the CFST stub columns in all the studied cases.

Obtained failure modes investigated in the parametric analysis are summarized in Fig. 10 for wall thickness 3 mm and 5.6 mm, respectively. The failure modes do not show significant differences by varying the material properties. The most significant difference is observed for structural steel grade S960 and concrete class C60/75 with wall thickness of 5.6 mm. In this case, a more notable plastic buckling shape develops around the end of the CFST stub column. On the other hand, smaller wall thickness of 3 mm results in less emphasised dimples around the inner quarter points.

Axial and hoop strains in the mid-height of specimens are also evaluated as examples for both normal and high strength steel tubes with wall thickness of 3 mm and 5.6 mm in order to represent different behaviours. Simulated strains in the reference point are presented in Fig. 11. It can be concluded that the presented normal strength steel CFSTs are capable of bearing loads without reduction of resistance until reaching 5% axial or hoop strains. On the other hand, high strength steel CFST with proof strength of 960 MPa showed a drop after buckling, then increase in load is observed. Wall thickness in this sense does not have an effect on strains in the mid-height of the specimen.

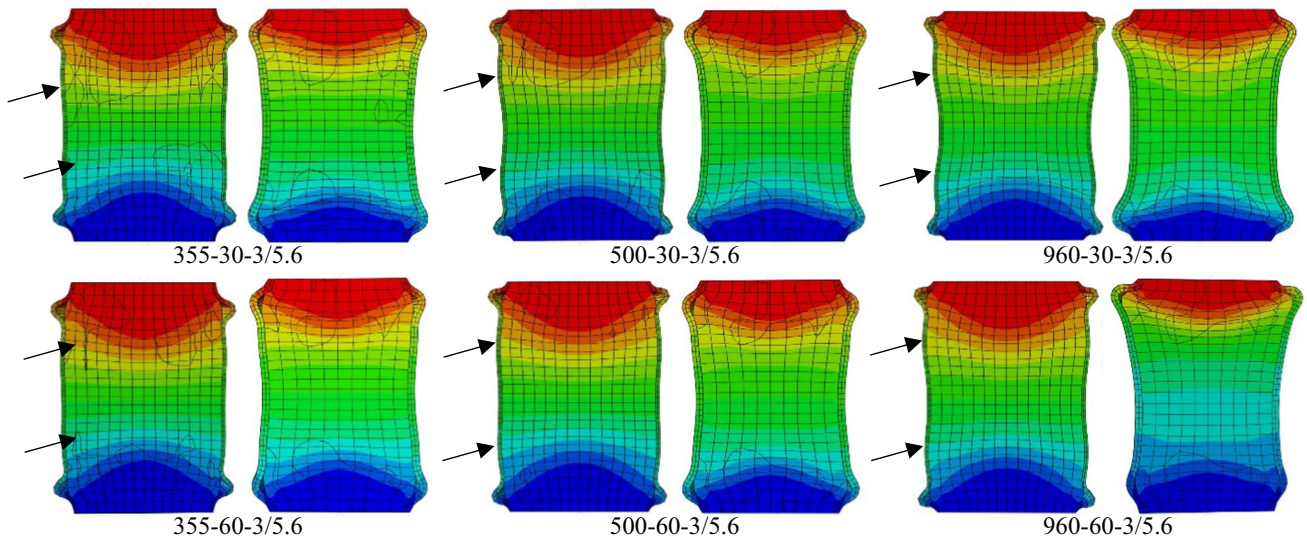

Fig. 10 Failure modes in the parametric analysis (extra dimples are denoted with arrows)

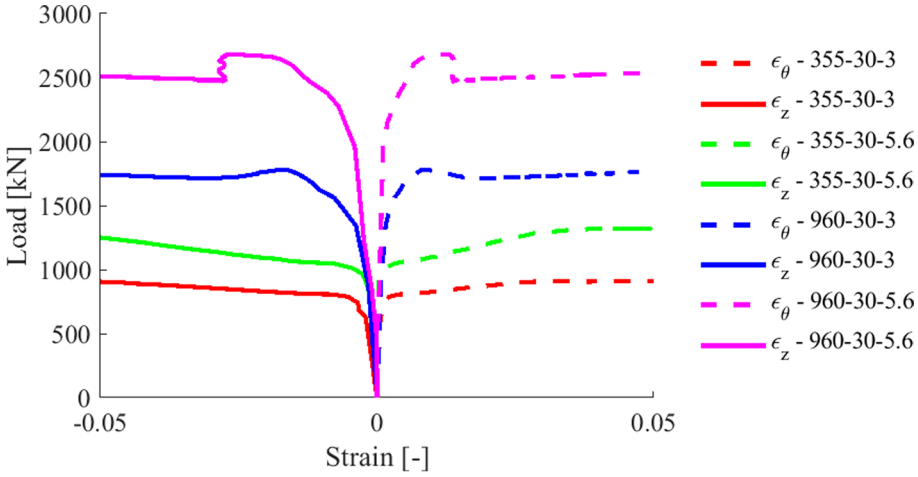

Fig. 11 Examples of axial (ε_z) and hoop (ε_θ) strains in the parametric analysis for CFSTs with normal and high strength steel tubes

Table 2 Load-bearing capacities [kN] of CFST specimens based on numerical modelling and design formulae

Specimen#	N_{theory}		$N_{ACI/AS}$		N_u		N_{Mander}		N_{EC}		$N_{proposal}$		N_{Num}	
310-60-3.1 (D167)	1713		1531		2079		1868		1504		1961		1880	
310-60-3.6 (D114)	925		844		1086		1037		900		1110		1088	
310-60-5.6 (D114)	1089		1014		1239		1246		1133		1356		1360	
355-30-3/5.6	646	926	605	889	729	1001	750	1085	765	928	800	1238	905	1230
500-30-3/5.6	798	1203	757	1165	880	1277	937	1411	790	1239	1051	1619	1130	1643
960-30-3/5.6	1279	2080	1238	2042	1362	2154	1514	2411	1349	2226	1659	2675	1826	2859
355-60-3/5.6	921	1175	839	1100	1086	1324	1032	1352	800	1096	1115	1504	1208	1489
500-60-3/5.6	1073	1452	990	1377	1238	1601	1224	1689	978	1409	1338	1897	1439	1903
960-60-3/5.6	1554	2329	1472	2254	1719	2478	1823	2733	1540	2399	1967	2996	2157	3118

The load-bearing capacities calculated using each design formula introduced in the literature review and numerical results (N_{Num}) are shown and summarised in Table 2 and Figs. 12 and 13 for each CFST stub column considered in the numerical analysis. The tabulated and plotted values are determined using the load factor for 5% principal strain according to EN 1993-1-5 since no maximum peak is observed in most of the modelled cases due to hardening of steel. Analytical calculations in this section consequently use characteristic compressive strength of concrete to represent the same design concept. Thus, analytical results can be compared with each other and with the numerical results as well. It affects only the Eurocode-based formula which basically uses the design strength of concrete. Comparison of the numerical results to the previous design proposals showed that the design method of Mander et al. gives the best approximation for the main part of the analysed cases. However, the analytically calculated compression resistance is always on the safe side, and it produces smaller compression resistance than provided by the numerical model. It is also observed that the difference increased by increasing the yield strength of the steel. Therefore, the formula of Mander et al. has been used as the base of the design method improvement.

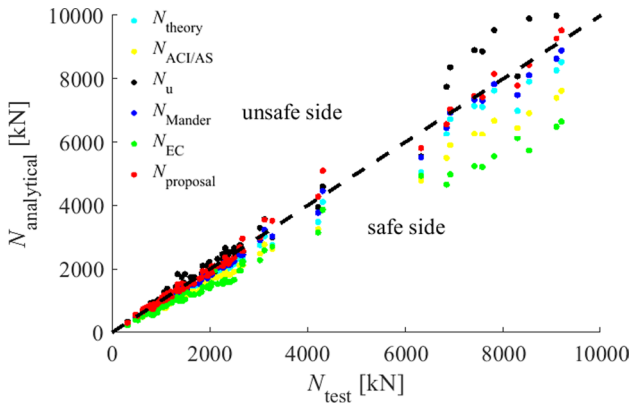

Fig. 12 Predicted analytical and test results based on the specimens gathered in Avci-Karatas, (2019)

A novel formula given by Eq. 15 is developed and proposed in the current paper to consider the behaviour of steel material more precisely. Hardening of steel is taken into account with steel stress at elongation equal to 5% (σ_{a5}) in accordance with EN 1993-1-5 and the evaluation of numerical results introduced above. The formulae of

prEN 1993-1-14 (2020), as given by Eqs. 9–14, are applied to capture yield plateau and strain-hardening behaviour of normal strength steels, while the Ramberg–Osgood material model, with $n = 14$ based on test results of Somodi (2018), are used for high strength steels (above yield strength of 360 MPa according to ISO TR 15608) to describe the stress–strain relationship presented in the current proposal. It yields $\sigma_{a5} = 368$ MPa, 435 MPa, 626 MPa and 1197 MPa for $f_y = 310$ MPa (validation), 355 MPa, 500 MPa and 960 MPa (parametric study), respectively. Confined compressive strength f_{cc} of concrete is also taken into consideration in order to include the increase of concrete compressive strength due to triaxial loading according to the formula (Eqs. 5–7) developed by Mander et al. (1989). Softening in concrete material model is ignored, while the proposed formula assumes that elastic shell buckling of the tubular section cannot occur. Thus, class 4 cross-section has to be avoided meaning that $D/t \leq 90\varepsilon^2$ needs to be fulfilled according to EN 1993-1-1 and EN 1993-1-12. The limit is $D/t = 59.4$ and 45.9 for S355 and S460, respectively.

$$N_{proposal} = A_a\sigma_a(5\%) + A_c f_{cc} \tag{15}$$

Errors, for different parameters, between analytical and numerical results are summarised in Table 3. It is unambiguous that numerical results are underestimated by all the formulae found in the literature. Based on the results, the ACI/AS recommendations ($N_{ACI/AS}$) and the theoretical load-bearing capacities (N_{theory}) based on the theory of composite structures have the lowest accuracy in all cases examined with an error of 9–33%. Formulae proposed by Giakoumelis and Lam (N_u) and Mander et al. (N_{Mander}) provide the best accuracy of 9–25% and 1–17%, respectively underestimating numerical load-bearing capacities. On the other hand, formula of Mander et al. is applicable for $t = 5.6$ mm, $f_{ck} = 60$ MPa and $f_y \leq 355$ MPa. Increasing either wall thickness or yield strength or decreasing compressive strength of concrete results in lower accuracy. It has to be highlighted that according to EN 1994-1-1, formulae of Eurocode (N_{EC}) can be applied only to CFSTs with steel grades up to S460 and normal weight concrete of strength classes up to C50/60 which is not the case for the analysed high strength steels (S500 and S960) and high strength concrete class (C60/75). However, deviations from numerical results are quite large even with using f_{ck} instead of f_{cd}; it underestimates numerical results with a minimum of 15% and a maximum of 34%. On the other hand, the proposed formula shows smaller deviations for all the analysed parameters and is specifically accurate for wall thickness $t = 5.6$ mm ($D/t = 20$) with deviation of 1–6% and for high strength materials.

A summary is made in tabular format (Table 4) consisting of all the analysed formulae and developed finite element model for comparing approximations in different aspects. Material behaviour and consideration of interaction between steel and concrete elements are compared in order to highlight the novelty and benefits of the proposed analytical formula.

A total of 104 specimens, summarized by Avci-Karatas (2019), and the corresponding experimental load bearing capacities are used for showing the accuracy of the analytical formulae, including the proposed equation. Only those test specimens are taken into consideration, out of 149 test specimens gathered in the referenced publication, in the evaluation of predicted load bearing capacities which are not susceptible to elastic shell buckling ($D/t \leq 90\varepsilon^2$). Specimen data including geometrical dimensions, material properties, experimental load bearing capacities and corresponding predicted values are available as supplementary material (Online Resource 1). The compressive strength of concrete varies between 18 and 193.3 MPa, while yield strength, or proof strength, varies between 248 and 853 MPa in the analysed experimental dataset. In the current paper, predicted analytical results ($N_{analytical}$) using different analytical formulae are shown in Fig. 12 with respect to test results (N_{test}).

Statistical evaluation of load bearing capacities for the specimens shown in Fig. 12 is summarized in Table 5. It is demonstrated that mean error for the proposed formula is much smaller than for the other analytical formulae on which the comparison is based. Standard deviation of errors is similar (4–6%) for the theoretical and ACI/AS standard-based formulae, the formula proposed by Mander et al., and the one proposed in the current paper. On the other hand, formulae proposed by Giakoumelis and Lam shows a larger variance (> 10%). Overall, the proposed formula is capable of determining load bearing capacities of CFSTs more accurately.

Table 3 Minimum and maximum errors [%] between analytical and numerical results, error = $(N_{analytical} - N_{Num})/N_{num} \times 100$

Analysed parameter	N_{theory}	$N_{ACI/AS}$	N_u	N_{Mander}	N_{EC}	$N_{proposal}$
$t = 3$ mm	−24 ÷ −30	−31 ÷ −33	−10 ÷ −25	−15 ÷ −17	−15 ÷ −34	−7 ÷ −12
$t = 5.6$ mm	−21 ÷ −27	−26 ÷ −29	−11 ÷ −25	−9 ÷ −16	−22 ÷ −26	−6 ÷ 1
$f_{ck} = 30$ MPa	−25 ÷ −30	−28 ÷ −33	−19 ÷ −25	−12 ÷ −17	−15 ÷ −30	−12 ÷ 1
$f_{ck} = 60$ MPa	−9 ÷ −28	−19 ÷ −32	−10 ÷ 10	−1 ÷ −16	−18 ÷ −34	−9 ÷ 4
$f_y \leq 355$ MPa	−20 ÷ −29	−25 ÷ −33	−9 ÷ −19	−8 ÷ −17	−15 ÷ −34	−8 ÷ 4
$f_y > 500$ MPa	−9 ÷ −30	−19 ÷ −33	-14 ÷ 10	−1 ÷ −17	−26 ÷ −32	−7 ÷ −9

Table 4 Comparison of approximations in analytical formulae and developed finite element model

Approach	Steel material	Concrete material	Confinement is considered	Contact between steel and concrete
Analytical formulae				
N_{theory}	Yield strength	Compressive strength on cube		Perfect
$N_{ACI/AS}$	Yield strength	Reduced compressive strength on cube due to uncertainties		Perfect
N_u	Yield strength	Increased compressive strength on cube due to confinement		Perfect
N_{Mander}	Yield strength	Compressive strength of confined concrete		Perfect
N_{EC}	Yield strength	Increased compressive strength on cube due to confinement		Perfect
$N_{proposal}$	Effective yield strength at 5% elongation	Increased compressive strength on cube due to confinement		Perfect
Developed finite element model	Isotropic hardening model	Isotropic hardening model, increased compressive strength on cube due to confinement		Standard frictional and tangential

Table 5 Statistical parameters of evaluated errors [%] between analytical and test results, error = $(N_{analytical} - N_{test})/N_{test} \times 100$

Statistical parameter	N_{theory}	$N_{ACI/AS}$	N_u	N_{Mander}	N_{EC}	$N_{proposal}$
Mean error μ [%]	−11.6	−18.8	2.9	−5.7	−22.5	0.5
Standard deviation of errors δ [%]	5.9	4.6	10.1	5.5	7.0	6.4
Coefficient of variation of errors δ/μ [–]	−0.5	−0.2	3.5	−1.0	−0.3	12.8
Minimum of errors [%]	−26.2	−29.5	−19.6	−19.0	−36.0	−11.2
Maximum of errors [%]	9.2	−4.9	37.4	11.7	−4.7	18.2

6 Conclusions

The application of both high strength materials and CFST columns are increasing in the civil engineering practice, but their combined application and performance in CFST columns still needed investigation. Therefore, nonlinear three-dimensional finite element models are developed for simulating the fundamental phenomena of concrete-filled steel tubes with circular hollow sections combining normal and high strength materials. The developed numerical model is validated based on test results and proved that it reliably captures the analysed physical phenomena and the load-carrying capacity. A total of twelve different CFST column configurations are investigated in the numerical parametric study using steel grades between S355–S960, concrete classes of C30/37 and C60/75 and *D/t* ratios of 20 and 38. Simulated compression resistances are compared to five different design models and the obtained tendencies are evaluated. Results showed that the proposal of Mander et al. showed the best approximation for the main part of the analysed cases; however, for increasing material strengths the difference between analytical and numerical results increased. Therefore, a novel design method, taking confined compressive strength of concrete and hardening of steel material into account in accordance with EN 1993-1-5, is proposed in the current paper to determine the compression resistance of CFST stub columns with a limitation of $D/t \leq 90\varepsilon^2$ (elastic shell buckling cannot occur). An experimental data set of 104 specimens found in the international literature is used for verifying the applicability and accuracy of the proposed approach along with existing analytical formulae. Statistical evaluation showed that the proposed new formula (Eq. 15) is capable of determining load bearing capacities of CFSTs more accurately than any other analytical approach. The data set consists of normal to high strength steels (f_y or $f_{p0.2} = 248 \div 853$ MPa), and normal to ultra-high performance concrete materials ($f_c = 18$ MPa $\div$ 193.3 MPa) covering a wide range of practical applications.

Supplementary Information The online version contains supplementary material available at https://doi.org/10.1007/s13296-022-00628-9.

Acknowledgements The presented research program has been financially supported by the Grant MTA-BME Lendület LP2021-06/2021 "Theory of new generation steel bridges" program of the Hungarian Academy of Sciences. The research reported in this paper and carried out at the Budapest University of Technology and Economics has been supported by the National Research Development and Innovation Fund (TKP2020 Institution Excellence Subprogram, Grant No. BME-IE-WAT) based on the charter of bolster issued by the National Research Development and Innovation Office under the auspices of the Ministry for Innovation and Technology. Financial supports are gratefully acknowledged.

Funding Open access funding provided by Budapest University of Technology and Economics.

References

Abed, F., AlHamaydeh, M., & Abdalla, S. (2013). Experimental and numerical investigations of the compressive behavior of concrete filled steel tubes (CFSTs). *Journal of Constructional Steel Research, 80*, 429–439. https://doi.org/10.1016/j.jcsr.2012.10.005

Abramski, M. (2018). Load-carrying capacity of axially loaded concrete-filled steel tubular columns made of thin tubes. *Archives of Civil and Mechanical Engineering, 18*, 902–913. https://doi.org/10.1016/j.acme.2018.01.002

Avci-Karatas, C. (2019). Prediction of ultimate load capacity of concrete-filled steel tube columns using multivariate adaptive regression splines (MARS). *Steel and Composite Structures, 33*, 583–594. https://doi.org/10.12989/scs.2019.33.4.583

Avci-Karatas, C. (2021). Modeling approach for estimation of ultimate load capacity of concrete-filled steel tube composite stub columns based on relevance vector machine Modeling approach for estimation of ultimate load capacity of concrete-filled steel tube composite stub colum. *Nigde Ömer Halisdemir University Journal of Engineering Science, 10*, 615–626. https://doi.org/10.28948/ngmuh.759297

Ayough, P., Ibrahim, Z., Sulong, N. H. R., & Hsiao, P.-C. (2021). The effects of cross-sectional shapes on the axial performance of concrete-filled steel tube columns. *Journal of Constructional Steel Research, 176*, 106424. https://doi.org/10.1016/j.jcsr.2020.106424

Canton tower. Retrieved March, 10, 2022, from https://www.klook.com/activity/2734-canton-tower-guangzhou/.

Dong, H., Li, Y., Cao, W., Qiao, Q., & Li, R. (2018). Uniaxial compression performance of rectangular CFST columns with different internal construction characteristics. *Engineering Structures, 176*, 763–775. https://doi.org/10.1016/j.engstruct.2018.09.051

Elchalakani, M., Zhao, X. L., & Grzebieta, R. H. (2001). Concrete-filled circular steel tubes subjected to pure bending. *Journal of Constructional Steel Research, 57*, 1141–1168. https://doi.org/10.1016/S0143-974X(01)00035-9

Ellobody, E., Young, B., & Lam, D. (2006). Behaviour of normal and high strength concrete-filled compact steel tube circular stub columns. *Journal of Constructional Steel Research, 62*, 706–715. https://doi.org/10.1016/j.jcsr.2005.11.002

EN 1994-1-1. Eurocode 4: Design of composite steel and concrete structures—Part 1–1: General rules and rules for buildings.

prEN 1993-1-14:2020. Eurocode 3: Design of steel structures, Part 1–14: Design assisted by Finite element analysis (under development by Committee for Standardization (CEN)).

Giakoumelis, G., & Lam, D. (2004). Axial capacity of circular concrete-filled tube columns. *Journal of Constructional Steel Research, 60*, 1049–1068. https://doi.org/10.1016/j.jcsr.2003.10.001

Han, L.-H., Li, W., & Bjorhovde, R. (2014). Developments and advanced applications of concrete-filled steel tubular (CFST) structures: Members. *Journal of Constructional Steel Research, 100*, 211–228. https://doi.org/10.1016/j.jcsr.2014.04.016

Han, L. H., Yao, G. H., & Tao, Z. (2007). Performance of concrete-filled thin-walled steel tubes under pure torsion. *Thin-Walled Structures, 45*, 24–36. https://doi.org/10.1016/j.tws.2007.01.008

Han, L.-H., Ye, Y., & Liao, F.-Y. (2016). Effects of core concrete initial imperfection on performance of eccentrically loaded CFST columns. *Journal of Structural Engineering, 142*, 04016132. https://doi.org/10.1061/(asce)st.1943-541x.0001604

Hassanein, M. F., Patel, V. I., & Bock, M. (2017). Behaviour and design of hexagonal concrete-filled steel tubular short columns under axial compression. *Engineering Structures, 153*, 732–748. https://doi.org/10.1016/j.engstruct.2017.10.010

He, A., Su, A., Liang, Y., & Zhao, O. (2021). Experimental and numerical investigations of circular recycled aggregate concrete-filled stainless steel tube columns. *Journal of Constructional Steel Research*. https://doi.org/10.1016/j.jcsr.2021.106566

Hu, H.-T., Huang, C.-S., Wu, M.-H., & Wu, Y.-M. (2003). Nonlinear analysis of axially loaded concrete-filled tube columns with confinement effect. *Journal of Structural Engineering, 129*, 1322–1329. https://doi.org/10.1061/(asce)0733-9445(2003)129:10(1322)

Huang, Y., Zhao, P., Lu, Y., & Zhang, H. (2022). Push-out tests of CFST columns strengthened with self-compacting and self-stressing concrete filled square steel tube. *Journal of Constructional Steel Research, 193*, 107263. https://doi.org/10.1016/j.jcsr.2022.107263

Ibañez, C., Hernández-Figueirido, D., & Piquer, A. (2021). Effect of steel tube thickness on the behaviour of CFST columns: Experimental tests and design assessment. *Engineering Structures, 230*, 111687. https://doi.org/10.1016/j.engstruct.2020.111687

Le, K. B., Van Cao, V., & Cao, H. X. (2021). Circular concrete filled thin-walled steel tubes under pure torsion: Experiments. *Thin-Walled Structures, 164*, 107874. https://doi.org/10.1016/j.tws.2021.107874

Li, N., Lu, Y., Li, S., & Gao, D. (2020). Axial compressive behaviour of steel fibre reinforced self-stressing and self-compacting concrete-filled steel tube columns. *Engineering Structures, 222*, 111108. https://doi.org/10.1016/j.engstruct.2020.111108

Mander, J. B., Priestley, M. J. N., & Park, R. (1989). Theoretical stress–strain model for confined concrete. *Journal of Structural Engineering, 114*, 1804–1826.

Michaleris, P. (2011). *Minimization of welding distortion and buckling*. Woodhead Publishing Limited.

Mursi, M., & Uy, B. (2003). Strength of concrete filled steel box columns incorporating interaction buckling. *Journal of Structural Engineering, 129*, 626–639. https://doi.org/10.1061/(asce)0733-9445(2003)129:5(626)

Patel, V. I., Hassanein, M. F., Thai, H. T., Al Abadi, H., Elchalakani, M., & Bai, Y. (2019). Ultra-high strength circular short CFST columns: Axisymmetric analysis, behaviour and design. *Engineering Structures, 179*, 268–283. https://doi.org/10.1016/j.engstruct.2018.10.081

Ren, Q. X., Han, L. H., Lam, D., & Li, W. (2014). Tests on elliptical concrete filled steel tubular (CFST) beams and columns. *Journal of Constructional Steel Research, 99*, 149–160. https://doi.org/10.1016/j.jcsr.2014.03.010

Romero, M. L., Espinós, A., Lapuebla-Ferri, A., Albero, V., & Hospitaler, A. (2020). Recent developments and fire design provisions for CFST columns and slim-floor beams. *Journal of Constructional Steel Research, 172*, 1–21. https://doi.org/10.1016/j.jcsr.2020.106159

Saenz, L. P. (1964). Discussion of paper "Equation for the stress–strain curve of concrete" by Desai and Krishnan. *Journal of the American Concrete Institute, 61*, 1229–1235.

Somodi, B. (2018). *Flexural buckling resistance of high strength steel welded and cold-formed square closed section columns*. Budapest University of Technology and Economics.

Tao, Z., Bin Wang, Z., & Yu, Q. (2013). Finite element modelling of concrete-filled steel stub columns under axial compression. *Journal of Constructional Steel Research, 89*, 121–131. https://doi.org/10.1016/j.jcsr.2013.07.001

Tretyakov, A., Tkalenko, I., & Wald, F. (2021). Fire response model of the steel fibre reinforced concrete filled tubular column. *Journal of Constructional Steel Research, 186*, 106884. https://doi.org/10.1016/j.jcsr.2021.106884

Concrete-Filled Steel Tube (CFST) bridges. Retrieved March, 10, 2022, from https://thereaderwiki.com/en/List_of_largest_arch_bridges.

La Vicaria bridge. Retrieved March, 10, 2022, from https://hu.wikipedia.org/wiki/Ívhíd#/media/Fájl:%0AVicaria_acabado.jpg.

Yan, J. B., Xie, W., Zhang, L., & Lin, X. C. (2019). Bond behaviour of concrete-filled steel tubes at the Arctic low temperatures. *Construction and Building Materials, 210*, 118–131. https://doi.org/10.1016/j.conbuildmat.2019.03.168

Yan, J.-B., Yang, X., Luo, Y., Xie, P., & Luo, Y.-B. (2021a). Axial compression behaviours of ultra-high performance concrete-filled Q690 high-strength steel tubes at low temperatures. *Thin-Walled Structures, 169*, 108419. https://doi.org/10.1016/j.tws.2021.108419

Yan, J. B., Yang, X., Luo, Y., Xie, P., & Luo, Y. B. (2021b). Axial compression behaviours of ultra-high performance concrete-filled Q690 high-strength steel tubes at low temperatures. *Thin-Walled Structures, 169*, 108419. https://doi.org/10.1016/j.tws.2021.108419

Ye, Y., Yao, X. H., & Guo, Z. X. (2021). Performance of concrete-filled stainless steel tubes subjected to concentric tension: Numerical investigation and parametric study. *Structures, 32*, 2222–2231. https://doi.org/10.1016/j.istruc.2021.04.028

Yu, M., Wang, T., Huang, W., Yuan, H., & Ye, J. (2019). Fire resistance of concrete-filled steel tube columns with preload. Part I: Experimental investigation. *Composite Structures, 223*, 110994. https://doi.org/10.1016/j.compstruct.2019.110994

Zhang, X., Chen, Y., Shen, X., & Zhu, Y. (2019). Behavior of circular CFST columns subjected to different lateral impact energy. *Applied Sciences, 9*, 1134. https://doi.org/10.3390/app9061134

Zhao, L., Cao, W., Guo, H., Zhao, Y., Song, Y., & Yang, Z. (2018). Experimental and numerical analysis of large-scale circular concrete-filled steel tubular columns with various constructural measures under high axial load ratios. *Applied Sciences, 8*, 1–21. https://doi.org/10.3390/app8101894